

## ORIGINAL ARTICLE

# Memory effect in elastic modulus of a hydrogen-bonding polymer network

Osamu Urakawa, Azusa Shimizu, Miho Fujita, Shun Tasaka and Tadashi Inoue

Dynamic networks constructed by physical cross-links between polymer chains can change their structure through the association and dissociation of cross-linking points. This paper yields experimental data about the transient change of the dynamic storage modulus  $G'$  for a molten random copolymer of vinyl acetate and vinyl alcohol with a vinyl alcohol content of 60 mol%, in which physical cross-links are formed via hydrogen bonding. As the cross-link density depends on temperature, the storage modulus  $G'$  of the system slowly evolves toward equilibrium at the experimental temperature,  $T_a$ , after changing the temperature from higher or lower than  $T_a$ . The characteristic time scale for the equilibration is on the order of  $10^3 \sim 10^4$  s (depending on  $T_a$ ) and the time evolution curves of  $G'$  are dependent on the thermal history. The 'memory effect' (the structure developed at a certain temperature is preserved after changing the temperature) found in the system is discussed in detail.

*Polymer Journal* (2017) 49, 229–236; doi:10.1038/pj.2016.113; published online 7 December 2016

## INTRODUCTION

Quenching a glass-forming system below its transition temperature,  $T_g$ , leads to a non-equilibrium state. Properties of the system slowly evolve toward equilibrium starting at the time quenched below  $T_g$ .<sup>1,2</sup> Such behavior can be seen in a variety of systems involving structural randomness, for example, in the dielectric and mechanical properties of polymeric glasses,<sup>3–6</sup> the magnetization of spin-glasses,<sup>7,8</sup> the folding structure of proteins,<sup>9</sup> the behavior of colloidal systems near the jamming transition<sup>10</sup> and the gelation of a gelatin system.<sup>11</sup> Despite the difference in their molecular-level structures, they commonly have various out-of-equilibrium meta-stable states and long equilibration times. The state or structure of systems evolved at a certain temperature,  $T_a$  ( $< T_g$ ), is known to be preserved to a certain degree even after a successive temperature change below  $T_a$ . This is called the memory effect and commonly appears in several random systems with many metastable states, although the detailed mechanism is still unclear. In this study, we present a preliminary result concerning the memory effect for a model random system that has not been investigated so far: a temporary network in which polymers are cross-linked to each other via hydrogen (H-) bonding interactions at temperatures far above  $T_g$ .

Inter-molecular H-bonds sometimes make materials solid, plastic-like or rubber-like even for non-polymeric systems.<sup>12–15</sup> In these cases, H-bonds have a role as temporal linkages of molecules, leading to the formation of a network structure. It is well known that the H-bond is a donor–acceptor interaction between a hydrogen atom and an electronegative atom, such as nitrogen or oxygen belonging to the chemical group of the same or a different molecule. The association energy of H-bonds ( $5 \sim 30$  kJ mol<sup>-1</sup> for OH··O) is stronger than the

van der Waals force but still weaker than ionic bonds or covalent bonds.<sup>16</sup> However, as the binding energy of H-bonds is higher than the thermal energy  $RT \sim 2.5$  kJ mol<sup>-1</sup> (at room temperature), this bond can survive for a long time at low temperatures.

Polymers bearing several H-bonding sites in the chain backbone are sometimes called 'sticky chain,' which can form linkages at multiple points.<sup>17,18</sup> In general, two types of H-bonds, namely, inter-chain and intra-chain H-bonds, are formed. Various combinations of these two types of H-bonds give rise to many possible structures having similar free energies. The multiple hydrogen bonds result in a prolonged lifetime of the associated structure, because all the hydrogen bonds rarely break up at the same time. As a result, the system will need a long time to reach a 'real' equilibrium state, hopping through many meta-stable structures. This situation is analogous to a glassy state and can thus be a model system to examine the intricate dynamics for frustrated random systems. The advantageous point of this system is that the equilibration time can be controlled by changing the chemical structure of the H-bonding site and/or its number in a polymer chain.

The physical gelation of the polymer solution reported by Parker and Normand<sup>11</sup> is a similar case that exhibits the memory effect related to network formation. They used gelatin gel in which the generation of a triple helix structure to serve as a cross-linking point triggers the gelation. However, the linkage structure of their system is complex, because the reversibility of association and dissociation by way of the coil  $\leftrightarrow$  helix transition is highly asymmetric compared to our system described below. In addition, the mechanical response will be affected by the rigid rod-like helix structure.

As a non-crystalline network-forming system, we used random-copolymers, poly(vinyl acetate-co-vinyl alcohol) with various

copolymer compositions, denoted as P(VA-OH), in which hydroxyl (OH) group can form hydrogen bonds (cross-linking points). In this study, the data are shown and discussed in detail only for P(VA-OH60), which has vinyl alcohol content,  $f_{\text{OH}} = 60$  mol%, and exhibits clear network forming behavior.

## EXPERIMENTAL PROCEDURE

P(VA-OH) samples were synthesized via a saponification reaction<sup>19</sup> of poly (vinyl acetate) with the molecular weight of  $M_w = 12\,000$  kDa and the distribution index,  $M_w/M_n = 1.77$ . Through this synthesis method, the degree of polymerization does not change ( $M_w = 12\,000$  kDa, meaning degree of polymerization = 140) and only the copolymer compositions can be varied. The molar fraction of OH groups (vinyl alcohol composition) to all the monomeric units,  $f_{\text{OH}}$ , and the randomness of the sequence distribution,  $\eta$ , were determined by the <sup>1</sup>H-nuclear magnetic resonance method.<sup>20,21</sup> The  $\eta$ -values for the VAc-VOH sequence were calculated from the following equation using the nuclear magnetic resonance intensities of the  $\alpha$ -proton in the polymer chain backbone:<sup>1</sup>

$$\eta = \frac{(\text{VOH}, \text{VAc})}{2f_{\text{OH}}(100 - f_{\text{OH}})} \quad (1)$$

Here, (VOH, VAc) represents a fraction of the neighboring unit of VOH and VAc.

Glass transition temperatures were determined by differential scanning calorimetry (DSC 6220, EXSTAR-6000, Seiko Instruments, Chiba, Japan) and the results are also shown in Table 1. Part of the sample characteristics are described elsewhere.<sup>22</sup> As well known, P(VA-OH) with high OH content is a semi-crystalline polymer. For the sample with the vinyl alcohol content ( $f_{\text{OH}}$ ) of 74%, which was not used in this study, an endothermic peak due to melting of the crystalline phase was observed in differential scanning calorimetry measurement. However, for P(VA-OH60), no melting peak was detected, meaning that the P(VA-OH) samples with  $f_{\text{OH}} \leq 60\%$  can be regarded as non-crystalline and amorphous materials. The differential scanning calorimetry data for P(VA-OH60) and P(VA-OH74) are compared in the Supplementary Figure S1 of the Supplementary Information.

For the examination of the hydrogen bonding structure in bulk P(VA-OH) samples, the infrared absorption (IR) spectra were measured with an IR spectrometer (Excalibur FTS 3000, Bio-Rad Laboratories, Chiba, Japan) using transmission method for the samples sandwiched between CaF<sub>2</sub> windows with the diameter of 20 mm and thickness of 1 mm. The temperatures were monitored by a thermocouple, which was set in the brass CaF<sub>2</sub> holder and controlled within  $\pm 0.2$  °C by a heating unit (homemade apparatus) being set in the spectrometer. For the temperature jump experiment, the time interval necessary for the temperature equilibration was about 1 min.

The rheological measurements were conducted by using ARES G2 (TA Instruments, Tokyo, Japan) equipped with 8 mm (diameter) parallel plates, except for creep experiment. The creep measurements were performed with MCR702 (Anton Paar, Tokyo, Japan) equipped with also 8 mm parallel plates. For both instruments, the temperatures of the bottom plate were monitored by a thermocouple and regarded as the sample temperatures.

**Table 1** Sample characteristics

Code	$f_{\text{OH}}/\text{mol}\%$	$\eta$	$T_g/\text{K}$
PVAc	2.0	—	308
P(VA-OH10)	10.1	0.81	309
P(VA-OH18)	18.0	0.79	311
P(VA-OH28)	27.8	0.58	313
P(VA-OH34)	34.5	0.53	317
P(VA-OH35)	35.4	—	319
P(VA-OH37)	37.4	—	319
P(VA-OH53)	53.3	0.30	—
P(VA-OH60)	59.9	0.50	323

## RESULTS AND DISCUSSION

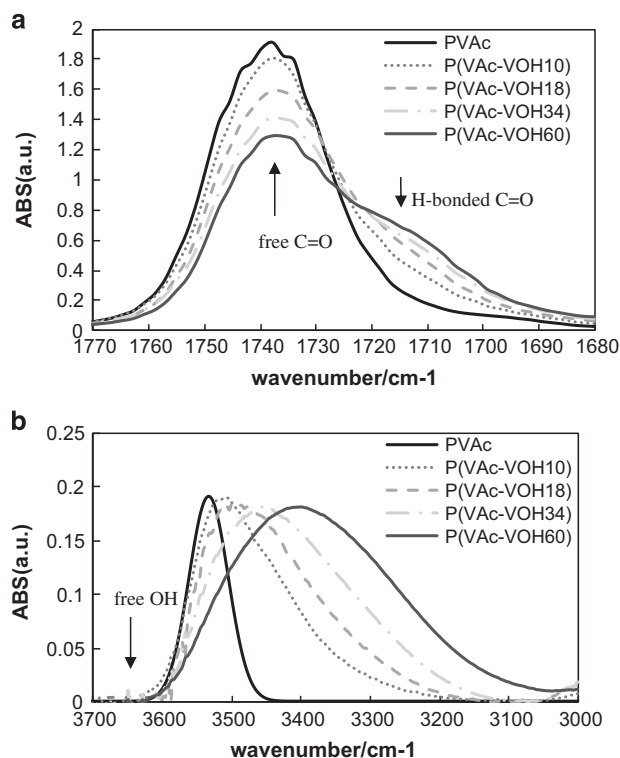
### Hydrogen bonding structure revealed by FTIR measurements

Figure 1 shows the FTIR absorbance spectra of (a) C=O stretching band (1770–1680 cm<sup>-1</sup>) and (b) OH stretching band (3660–3040 cm<sup>-1</sup>) measured at 30 °C for various P(VA-OH) samples. With the increase of the OH content,  $f_{\text{OH}}$ , the H-bonded C=O observed at around 1716 cm<sup>-1</sup> as a shoulder of the main peak located at 1735 cm<sup>-1</sup> (free C=O) increases. These spectra were separated into two peaks corresponding to the free and H-bonded C=O, and the molar ratio of these components were determined from the peak intensities by following the procedure described in the textbook.<sup>23</sup> The details of this analysis is shown in the Supplementary Information 2.

Concerning the OH stretching band, we found that free (non-H-bonded) OH did not exist in the bulk state. The free OH peak was confirmed to appear at around 3660 cm<sup>-1</sup> for toluene solution of P(VA-OH10). These results indicate that all the OH groups are bonded to the C=O or other OH groups in the molten P(VA-OH) samples. In addition, the shape of the OH stretching band broadens toward lower wave numbers with increasing  $f_{\text{OH}}$ , suggesting the formation of the H-bonded structures with multiply-connected OH groups (OH...OH...OH...) and its multiplicity increases with  $f_{\text{OH}}$ .

From the molar contents of free or H-bonded C=O groups, we determined the fraction of the OH groups which are H-bonded with C=O or other OH groups based on the assumption that there exists no free OH group. The result is shown in Figure 2, which indicates that the H-bonded structure in the P(VA-OH) systems mainly consists of the OH...OH connected species.

Figure 3 shows the temperature dependence of (a) C=O stretching, and (b) OH stretching spectra for P(VA-OH60). As seen in Figure 3b, even at high temperature, no free OH peak appears at around



**Figure 1** FTIR spectra of (a) C=O stretching band and (b) O-H stretching band in bulk P(VA-OH)s with various OH content and PVAc (containing a few % OH group). A full color version of this figure is available at *Polymer Journal* online.

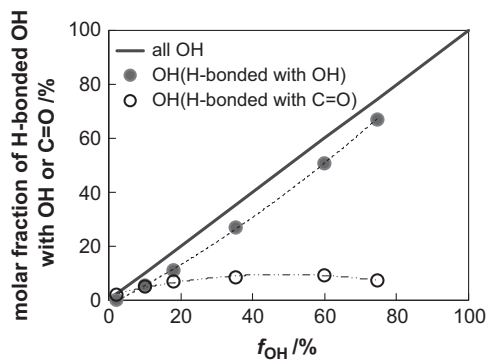


**Figure 2**  $f_{\text{OH}}$  dependence of the molar fraction of hydrogen bonded OH with OH or C=O groups at 30 °C. A full color version of this figure is available at *Polymer Journal* online.

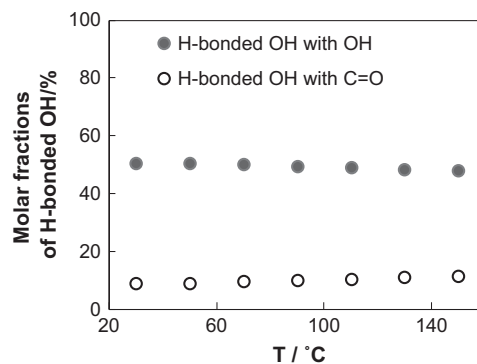


**Figure 4** Temperature dependence of the molar fraction of hydrogen bonded OH with OH or with C=O groups for P(VA-OH60). A full color version of this figure is available at *Polymer Journal* online.

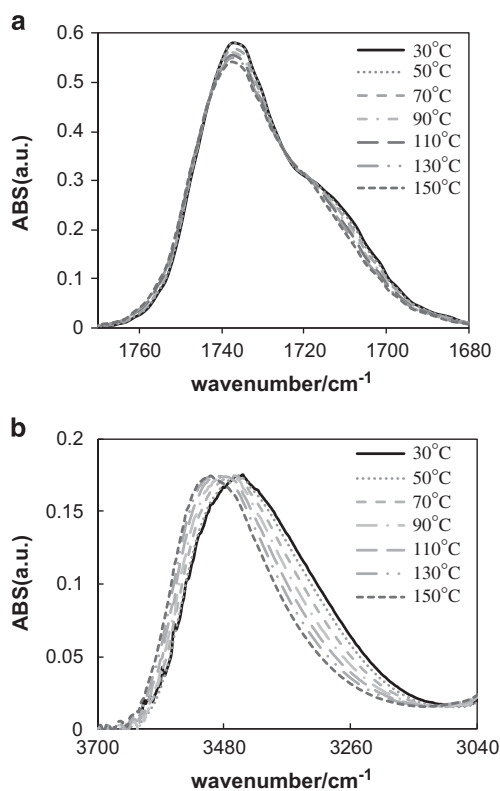


**Figure 3** FTIR spectra for (a) C=O stretching and (b) O-H stretching bands of P(VA-OH60) at various temperatures. A full color version of this figure is available at *Polymer Journal* online.

$3660\text{ cm}^{-1}$ . Therefore, by analyzing the C=O spectra (see Supplementary Information 2), the H-bonded species were determined in the same way as done in Figure 2. The result is shown in Figure 4. It is seen that the fraction of H-bonding species for the OH group is insensitive to the temperature. However, Figure 3b clearly indicates the change in the spectral shapes for OH stretching band, suggesting the decrease in the length (multiplicity) of the linearly connected OH groups, as schematically shown in Figure 5.

Figure 6 compares the FTIR spectra just before and after the temperature drop from 150 °C to 120 °C and after 5400 s annealing at 120 °C for (a) C=O and (b) O-H stretching bands. It is seen that the FTIR data measured at  $t \sim 0$  s and  $t \sim 5400$  s are almost identical for

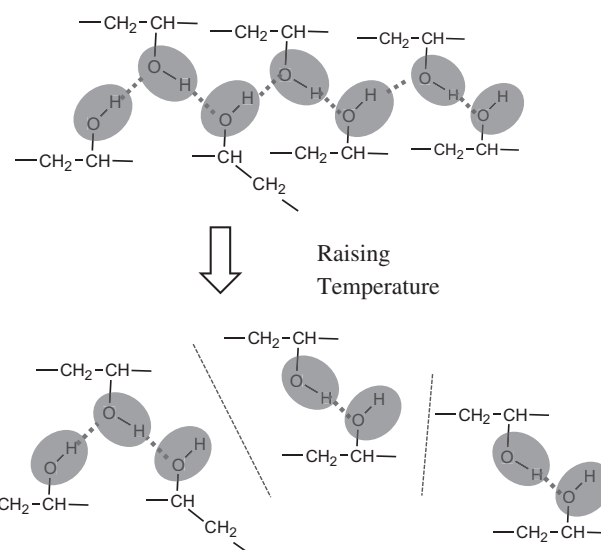


**Figure 5** Schematic illustration of the change in the OH...OH multiple H-bonding structure in P(VA-OH) samples. A full color version of this figure is available at *Polymer Journal* online.

both OH and C=O stretching bands. For the temperature change of the IR sample holder it takes about 1 min and for taking the IR data it also takes about 1 min, meaning the time resolution of this measurement is on the order of  $10^2$  s. For C=O spectra, its shape is almost unchanged by changing the temperature, so that the time evolution of the H-bonding structure cannot be discussed from this data. However, for OH band, the shape of IR spectrum certainly changes after temperature drop and the data at  $t \sim 0$  s (with the resolution of 100 s) and  $t \sim 5400$  s are the same, meaning that the change of the IR spectra is faster than  $10^2$  s and the H-bonding structure revealed by this measurement reach equilibrium within  $10^2$  s. As will be discussed in the next section (in Figure 8), rheological data exhibit much slower change. Concerning the difference in the time evolution behavior between IR and rheology data, our interpretation will be described in the following section.

#### Rheological behavior (memory effect)

Supplementary Figure S3 in the Supplementary Information summarizes the rheological data: the frequency,  $\omega$ , dependence of the shear storage modulus,  $G'(\omega)$ , of P(VA-OH)s having various  $f_{\text{OH}}$ . We used the method of reduced variables (temperature–frequency

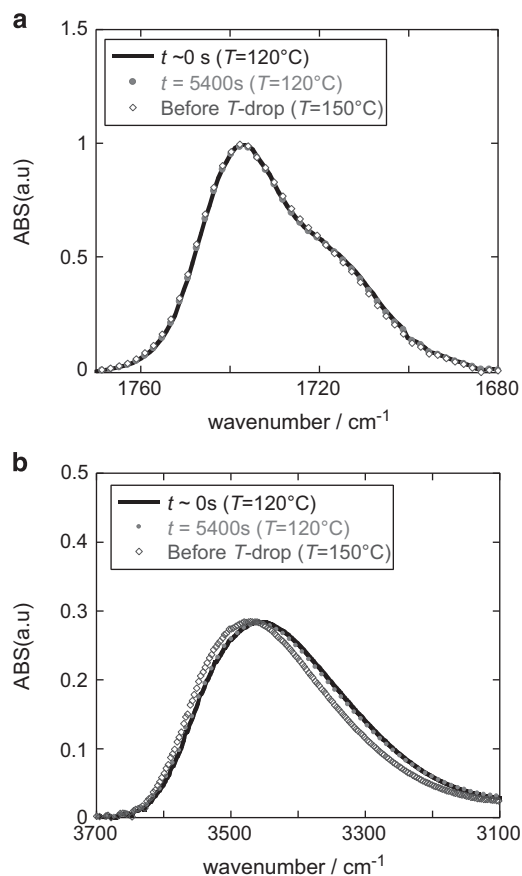


**Figure 6** Comparison of absorption spectra at 150 °C and after the temperature drop to 120 °C at  $t \sim 0$  s and 5400 s, for (a) C=O stretching and (b) OH stretching bands. The data at  $t \sim 0$  s were taken after the temperature of the FTIR sample holder having reached  $T = 120 \pm 0.5$  °C. It took about 1 min for changing temperature. Moreover, to take the spectrum data (32 times averaging) it also takes about 1 min. Therefore, there is an ambiguity in the time scale on the order of  $10^2$  s. A full color version of this figure is available at *Polymer Journal* online.

superposition principle)<sup>24</sup> to construct the composite curve of  $G'$  for each sample. The deviation from the Rouse spectrum shown by the solid curves can be seen at low  $\omega$  for  $f_{\text{OH}} \geq 34\%$  and becomes more pronounced with increasing the OH content. For the P(VA-OH53) and P(VA-OH60) samples the superposition principle clearly fails at the low  $\omega$  region. The plateau region ( $G'(\omega) \sim \text{constant}$ ) at low  $\omega$  clearly appears for the P(VA-OH60) and the intensity of the plateau level increases by lowering the temperature. The  $G'$  curves of P(VA-OH60) is separately shown in Figure 7a. The superposition works only at high frequency regions because the high  $\omega$  response corresponds to the chain relaxation. In contrast, the data at low  $\omega$ , which reflect the network structures formed by H-bonding, are strongly dependent on temperature. As the magnitude of the low-frequency modulus  $G_N$  decreases with increasing temperature, it can be said that the cross-linking density decreases with temperature. At  $T = 120$  °C, the  $G_N$  value was determined to be  $3.2 \times 10^2$  Pa by subtracting the high frequency chain relaxation component. Such low  $G_N$  value suggests that the effective cross-linking density is very low and the network strand does not consist of a portion of polymer chain but aggregates of a large number of polymer chains. In this molten system, there is considerable overlapping of polymer chains and thus the mean field approximation is applicable.<sup>17,18</sup> The aggregation

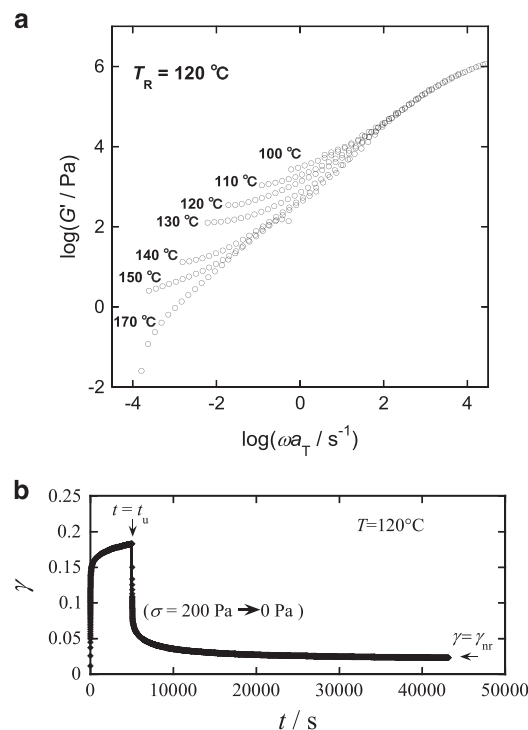


**Figure 7** (a) Composite curve of storage modulus  $G'(\omega)$  for molten P(VA-OH60) superposed in the high frequency region. The reference temperature is 120 °C. (b) Time dependence of shear strain during the creep and creep recovery test. Constant strain ( $\sigma = 200$  Pa) was applied at  $t = 0$ , and unloaded at  $t = t_u = 5.05 \times 10^3$  s.

number of polymer chains involved in one effective strand (real backbone strand), except for the branched and dangling part,  $N_{\text{strand}}$  can be estimated from the relation of  $N_{\text{strand}} \sim (\rho RT / G_N M_w)^{1/3}$  (predicted by the sticky Rouse model),<sup>18</sup> where  $R$  is the gas constant,  $\rho$  is the density and  $M_w$  is the molecular weight of P(VA-OH). From this equation  $N_{\text{strand}} \sim 11$  was obtained, meaning that 11 chains are involved in one effective network strand.

To check whether the network structure in this system is dynamic or static, we conducted creep and creep recovery test for P(VA-OH60) at 120 °C. The result is shown in Figure 7b. The applied stress  $\sigma_0$  in the creep experiment ( $0 < t < t_u = 5.05 \times 10^4$  s) was 200 Pa, which is low enough for this system to be in the linear regime. It is seen that in the creep recovery process ( $t > t_u$ ) the strain does not recover to zero even after  $4.3 \times 10^4$  s. This non-recoverable strain,  $\gamma_{\text{nr}}$ , is caused by the flow of the sample during the creep experiment. This result means that this system can be regarded as 'viscoelastic liquid' and the plateau region of  $G'$  observed in Figure 7a is expected to decrease to zero at lower frequency than that corresponding to the life time of this temporal network. The zero shear viscosity  $\eta_0$  can be estimated from the unrecovered strain ( $\eta_0 = \sigma_0 t_u / \gamma_{\text{nr}}$ ) to be  $4.3 \times 10^7$  Pas and the relaxation time  $\tau_{\text{term}}$  can also be estimated to be  $3.8 \times 10^4$  s from the  $\eta_0$  and the recoverable compliance  $J_R (= 8.8 \times 10^{-4} \text{ Pa}^{-1})$  as  $J_R \eta_0$ .

Reflecting such long relaxation time, the  $G'$  value slowly changes after changing temperature. Supplementary Figure S4 in the Supplementary Information compares the data just after the temperature change from 150 to 120 °C and after nearly equilibration at 120 °C. Although the high  $\omega$  data are identical, the low  $\omega$  plateau is found to increase slowly through the equilibration process. This means that network density gradually increases with time. To investigate the

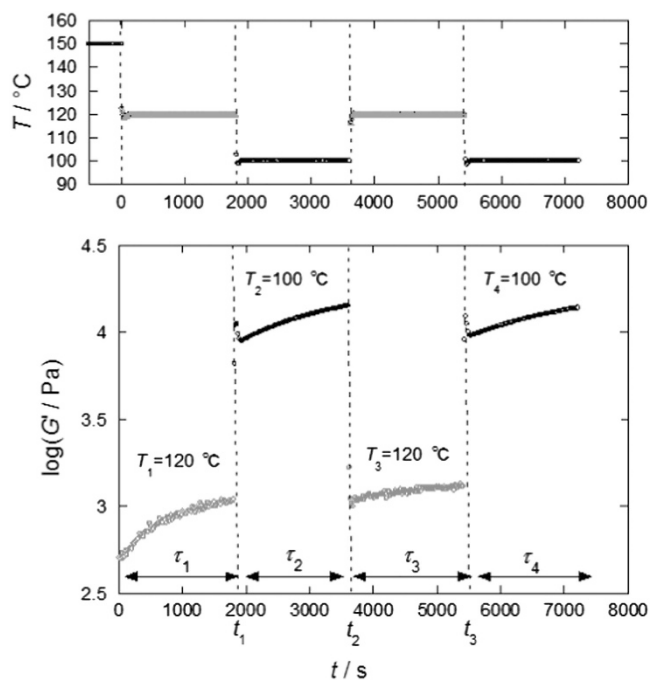


**Figure 8** Typical thermal history applied to the P(VA-OH60) sample (upper figure) and time evolution of  $G'$  (at  $\omega = 1 \text{ s}^{-1}$ ) accompanied by such temperature changes (lower figure). Here,  $\tau_1 = \tau_2 = \tau_3 = \tau_4 = 1800 \text{ s}$ . A full color version of this figure is available at *Polymer Journal* online.

kinetics of the network formation, we monitored the  $G'$  value at  $\omega = 1 \text{ s}^{-1}$  as a function of time after temperature changes for P(VA-OH60). The result is shown in Figure 8 together with the protocol of temperature change (time dependence of the actual sample temperature is shown in the upper figure). First, the sample was equilibrated at 150 °C, and the temperature was changed to 120 °C ( $T_1$ ). After that,  $G'$  increased and gradually approached a new equilibrium value. As the characteristic time of the thermostatic convection oven of the rheometer is less than 1 min (as show in the upper figure), the slow evolution of  $G'$  certainly reflects the structural change of the hydrogen-bonding network.

It is noteworthy that after the  $T$ -drop the shape of the FTIR spectra reached equilibrium rapidly (within  $10^2 \text{ s}$ ; see Figure 6). To explain the different time evolution behavior between FTIR and rheology, we think the ratio of intra- to inter-molecular H-bond will be an important factor. FTIR cannot distinguish two types of H-bond, while the rheological ( $G'$ ) measurement detects the latter emphatically. Therefore, the different time evolution behavior could be explained by assuming the following possible structural change. After the  $T$ -drop, intra-molecular association will be preferably formed in non-equilibrium state due to quick bond formation mostly between the nearest pair of OH groups, which stochastically belong to the same chain and then gradually switches to inter-molecular association without changing the number of H-bonds. We think that there is a certain equilibrium number ratio of the intra- to inter-chain association at each temperature; however, just after the  $T$ -change, an intra-chain rich H-bonding structure will be temporarily formed by a kinetic reason. Such temporary structure may be slightly unstable, because the formation of intra-chain bonds will make single chain conformation more compact and non-Gaussian like, resulting in slightly higher energy state. Such energy difference can be the driving force to switch from intra- to inter-chain H-bonds. The volume

fraction of OH groups belonging to the different chain around one OH group will be high enough in the molten P(VA-OH60) system to form inter-chain H-bond.

Concerning the lifetime of H-bonds, it is reported that rearrangement time of hydrogen bonding network in water is on a picosecond time scale.<sup>25</sup> Even by considering our system is undiluted and has lower mobility compared with bulk water, the terminal time of P(VA-OH60) seems to be much longer than the lifetime of individual hydrogen bonds. This will be due to the multiple H-bonds formed in polymeric system. Several polymer chains zip together via multiple H-bonds, and would need to break many H-bonds at the same time to relax. For further quantitative discussion, we have to wait until knowing the individual lifetime of H-bonds somehow by some experimental methods such as transient IR spectroscopy.

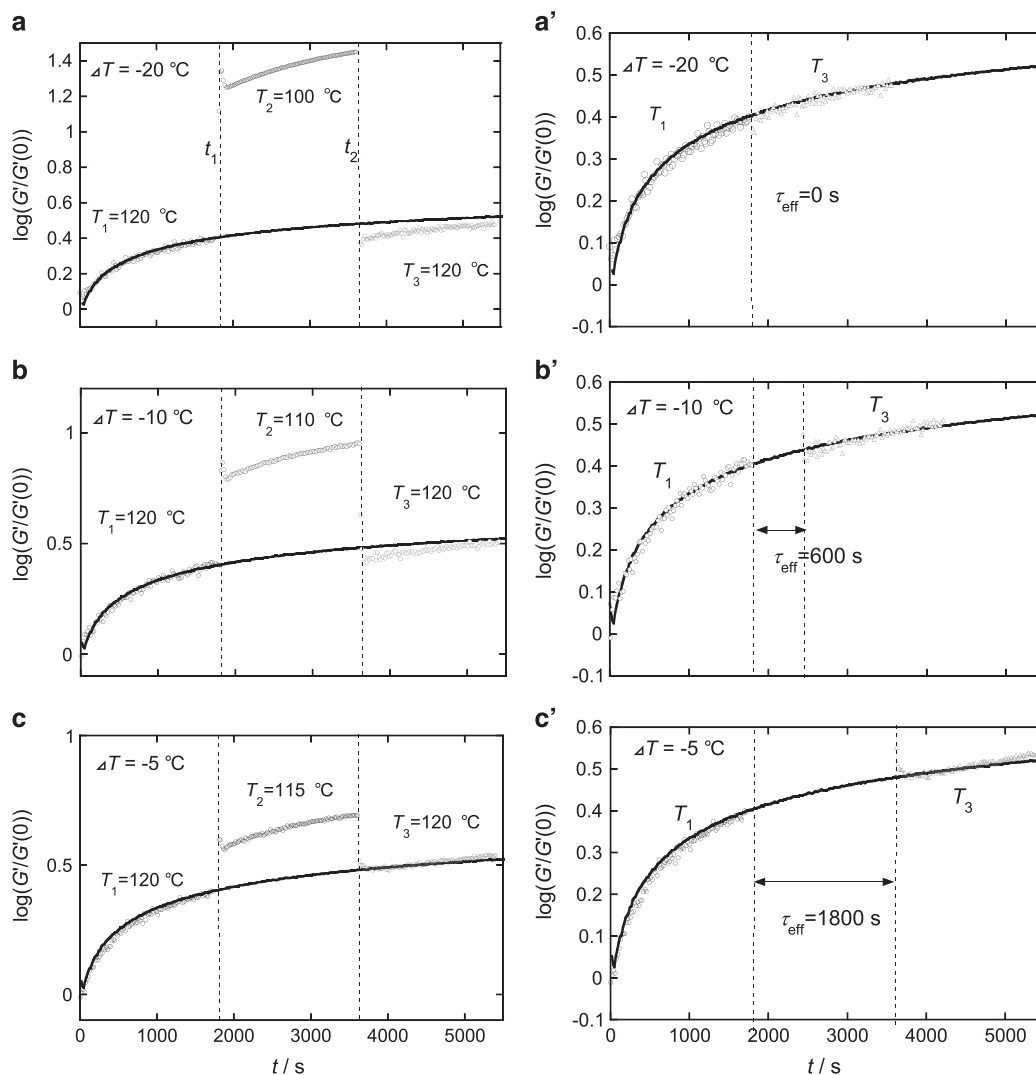
As shown in Figure 8, the annealing period at  $T_1$ , denoted as  $\tau_1$ , was 1800 s. After the second temperature drop to 100 °C ( $T_2$ ),  $G'$  increased instantaneously and subsequently changed toward a new equilibrium state. The instant change of  $G'$  after the  $T$ -drop is mainly caused by the change in the chain relaxation component (change in the friction factor), which increases the  $G'$  by  $\sim 1$  decade at  $\omega = 1 \text{ s}^{-1}$ . When the successive temperature change jumped to 120 °C ( $T_3$ ),  $G'$  decreased instantaneously and then gradually increased. If the magnitude of the plateau modulus reflecting the cross-linking density is simply determined only by temperature,  $G'$  should monotonically decrease after this temperature change from 100 to 120 °C. The present results indicate that the magnitude of the plateau modulus is determined in a more complicated way depending on the thermal history. A network structure evolved at 120 °C ( $T_1$ ) in the first aging process is retained, and the annealing at 100 °C ( $T_2$ ) seems to have no effect on that structure because in the third annealing process at 120 °C ( $T_3$ ), the  $G'$  value starts to increase from the point reached in the first aging at 120 °C ( $T_1$ ). In the fourth annealing process at 100 °C ( $T_4$ ),  $G'$  traces almost the same time dependence as in the 2nd annealing process at 100 °C ( $T_2$ ). This means that high temperature annealing at 120 °C ( $T_3$ ) completely erases the memory of the structure evolved at the  $T_2$  annealing.

Figure 9 shows the results of aging experiments varying the temperature of the second annealing,  $T_2$  (100 °C (a), 110 °C (b) or 115 °C (c)). The result of long time annealing at 120 °C, which corresponds to  $T_1 = T_2 = T_3 = 120 \text{ °C}$ , is also shown in these figures by solid curves. The 120 °C annealing data can be experimentally fitted by the sum of two retardation functions.

$$\frac{G'(t)}{G'(0)} = \sum_{i=s,l} \bar{G}_i \left( 1 - \exp\left(-\frac{t}{\tau_i}\right) \right) \quad (2)$$

The parameters in this equation were determined to be  $\bar{G}_S = 0.938$ ,  $\tau_s = 444 \text{ s}$ ,  $\bar{G}_l = 2.22$  and  $\tau_l = 4540 \text{ s}$ . It is worth noting that  $\tau_l$  is one order shorter than the terminal time  $\tau_{\text{term}}$  ( $3.8 \times 10^4 \text{ s}$ ) estimated from the creep experiment. This is possibly because the retardation component corresponding to the terminal time cannot be detected by this shorter time experiment.

By shifting the time evolution curve of the third annealing (at  $T_3$ ) along the horizontal axis by the amount  $t_{\text{shift}}$ , the  $G'$  curves of the first and third annealing are smoothly connected and almost coincide with the  $G'(t)$  curve measured at 120 °C continuously, which is shown by the solid line (see the Figures 9a'–c'). Here, the interval time  $\tau_{\text{eff}}$  is defined as  $\tau_{\text{eff}} = t_2 - t_1 - |t_{\text{shift}}|$  ( $= 1800 \text{ s} - |t_{\text{shift}}|$ ) and was determined to overlap the  $T_3$  annealing data with the solid curve. Increasing  $T_2$  (decreasing  $\Delta T \equiv T_1 - T_2 > 0$ ) induces an increase of the interval time  $\tau_{\text{eff}}$  as shown in Figure 9. This means that the network structure evolved during  $T_1$ -annealing continues to develop at  $T_2$  if  $\Delta T$  is small.



**Figure 9** Time evolution of  $G'$  measured at  $\omega = 1 \text{ s}^{-1}$  for P(VA-OH60) under several thermal histories. The vertical axes are reduced by  $G'(0)$ , which is the initial value at  $t=0$ . Here,  $t_1 = 1800 \text{ s}$ ,  $t_2 = 3600 \text{ s}$  and  $\Delta T = T_1 - T_2$ . Here  $\Delta T = 20 \text{ }^\circ\text{C}$  (a),  $10 \text{ }^\circ\text{C}$  (b) and  $5 \text{ }^\circ\text{C}$  (c). The solid curves indicate the single temperature annealing results at  $120 \text{ }^\circ\text{C}$ . In the right-hand side figures,  $a'$ ,  $b'$  and  $c'$ , the  $G'$  curves at  $T_3$  were superposed on the solid (single temperature annealing) curve by a horizontal left shift with  $t_{\text{shift}} = t_2 - t_1 - \tau_{\text{eff}}$ . A full color version of this figure is available at *Polymer Journal* online.

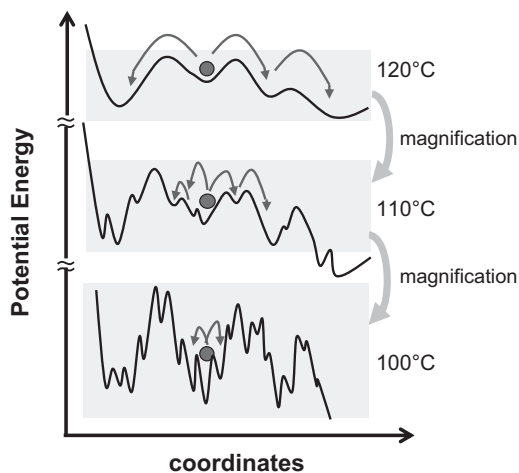


**Figure 10** Schematic illustration of energy landscapes, which are drawn with different enlargement factors at each temperature. A full color version of this figure is available at *Polymer Journal* online.

Conversely, if  $\Delta T$  is large, the network formations at  $T_1$  and  $T_2$  become independent. Therefore, the independence of the structural evolution between  $T_1$  and  $T_2$  only appears when  $\Delta T$  is large ( $\geq 20 \text{ }^\circ\text{C}$ ).

In the Supplementary Information (Supplementary Figure S5), similar data measured under different conditions are shown: lower frequency ( $\omega = 0.1 \text{ s}^{-1}$ ), higher temperatures ( $130 \text{ }^\circ\text{C} \rightarrow 110 \text{ }^\circ\text{C} \rightarrow 130 \text{ }^\circ\text{C}$ ) and longer annealing periods ( $\tau_1 = \tau_2 = \tau_3 = 8000 \text{ s}$ ). In essence, the same result as those described above was observed, meaning that the experimental conditions shown in Figures 8 and 9 are not crucial to see the memory effect.

At high temperature, a loose network with a low cross-linking density is formed. Such a structure will be entropically more stable than that formed at a lower temperature due to the relaxed conformation of each chain and also each network strand resulting from the lower number of H-bonded points and higher mobility. Such a free-energy difference will be essential for the appearance of the memory effect. When the temperature is dropped to  $T_2$ , new H-bonds are created between the nearest pair of O and OH groups. Among them, partially unstable (frustrated) structures are incorporated. The

formerly constructed stable structures at  $T_1$  will not change so easily even though new H-bonds are added in the system at  $T_2$ . Through the equilibration process at  $T_2$ , newly formed H-bonds will be easily broken up and reformed in the system, gradually evolving to a more stable structure by preserving the old (stable) H-bonding parts. Moreover, at  $T_2$ , the equilibration time becomes longer than that at  $T_1$  due to the higher cross-linking density and lower molecular mobility; accordingly, the change of the stable H-bonding structure becomes harder. Because of such a kinetic effect, the stable structure formed at  $T_1$  is largely preserved during the  $T_2$ -annealing. After the next temperature change from  $T_2$  to  $T_3$  ( $=T_1$ ), the unstable structure is selectively broken, and the stable one becomes observable. We think this is the possible mechanism of the appearance of the memory effect.

Such behavior can be qualitatively explained with an energy landscape picture.<sup>26,27</sup> In fact, we have not probed directly the detailed aggregation structure of the H-bonding network and thus it is noted that the following explanation is just a visualization of our assumption. Figure 10 schematically shows the potential energy surfaces for H-bonding networks as a function of the coordinates specifying the position of all molecules. To emphasize the temperature effect, the energy profiles, which should be the same at different temperatures, are drawn more enlarged at lower temperatures. The depths of energy wells correspond to the barrier to change the total H-bonding structure of the system, for example, to break the slight unstable (probably intra-chain) H-bonds. The adjacent minimum corresponds to the formation of more stable (probably inter-chain) H-bond. At lower temperatures, both the number of local minimums and their depths looks higher for the system because of the lower thermal energy (driving force) to change the structure. The possible changes of the states with time are depicted by blue thin arrows in this figure: during the annealing at 100 °C, the system is trapped around the deep basin where the system reached in the first annealing at  $T_1$  (120 °C). After the temperature jump from 100 °C ( $T_2$ ) back to 120 °C ( $T_3$ ), the state starts moving again from the original point. Conversely, in the case of  $T_2=110$  °C, the system changes toward the more stable structure during the  $T_2$ -annealing, and thus, the state of the system had evolved when back to  $T_3=120$  °C (resulting in a weaker memory effect).

A similar memory effect was reported to appear in the time evolutions of dielectric permeability for glassy polymers<sup>5</sup> and of volume for granular compaction.<sup>10</sup> Cooling the materials below the glass transition temperature, they solidify and retain structural disorder. Slow structural change occurs to increase molecular packing. This evolution process will be driven through the hopping among several meta-stable states as shown in Figure 10. Even for completely different materials, including the present system, all of them possess frustrated structures, and thus, a similar energy landscape picture can be drawn. This scenario for the appearance of the memory effect suggests the universal feature in random frustrated systems.

## CONCLUSION

We examined the structure and dynamics of non-entangled random copolymer of vinyl acetate and vinyl alcohol, P(VA-OH), in which hydrogen bonding interaction plays a role. Among the samples with different copolymer compositions, the P(VA-OH60) with the OH content of 60% exhibited clear plateau region in the storage modulus due to the temporal hydrogen bonding network structure. FTIR measurements on the molten P(VA-OH) systems revealed that the major component of the H-bonding structure was OH...OH bond (the OH...O=C bond was minor). It has been considered that this

type of hydrogen bonds formed between different polymer chains will be the main cause of the network formation.

By changing the temperature of the bulk P(VA-OH60) equilibrated at 150–120 °C, the  $G'$  value changed slowly toward new equilibrium on the time scale longer than  $10^3$  s. On the other hand, the FTIR spectra changed much faster (faster than  $10^2$  s) compared with the case of  $G'$ . The long evolution time of the  $G'$  was ascribed to the change of the H-bonding structure from the intra-chain to the inter-chain one.

Concerning the time evolution of the plateau modulus for the molten P(VA-OH60) system, we observed the memory effect; The  $G'$  value developed at 120 °C was preserved after annealing at 100 °C and getting back to 120 °C. For the appearance of this type of memory effect, the formation of the frustrated H-bonding structure and its stability difference at different temperatures were considered to be the key factors. From the analogy with the glass forming system, we concluded that the temporal cross-linking via H-bonds had a similar effect as the densification of glassy materials on the structural evolution

## CONFLICT OF INTEREST

The authors declare no conflict of interest.

## ACKNOWLEDGEMENTS

This work was supported by JSPS KAKENHI Grant Number 21350126.

- 1 Struik, L. C. E. *Physical Aging in Polymers and Other Amorphous Materials* (Elsevier, Amsterdam, 1978).
- 2 Angell, C. A., Ngai, K. L., McKenna, G. B., McMillan, P. F. & Martin, S. W. Relaxation in glassforming liquids and amorphous solids. *J. Appl. Phys.* **88**, 3113–3157 (2000).
- 3 Bellon, L., Ciliberto, S. & Laroche, C. Advanced memory effects in the aging of a polymer glass. *Eur. Phys. J. B* **25**, 223–231 (2002).
- 4 Wang, X. R. Time-temperature independence of aging-induced relaxation peak in the glassy state. *Macromol. Rapid Commun.* **23**, 530–534 (2002).
- 5 Fukao, K. & Sakamoto, A. Aging phenomena in poly(methyl methacrylate) thin films: memory and rejuvenation effects. *Phys. Rev. E* **71**, 041803-1-12 (2005).
- 6 Cavaille, J. Y., Etienne, S., Perez, J., Monnerie, L. & Johari, G. P. Dynamic shear measurements of physical aging and the memory effect in a polymer glass. *Polymer* **27**, 686–692 (1986).
- 7 Jonason, K., Vincent, E., Hammann, J., Bouchaud, J. P. & Nordblad, P. Memory and chaos effects in spin glasses. *Phys. Rev. Lett.* **81**, 3243–3246 (1998).
- 8 Nordblad, P. Spin glasses: model systems for non-equilibrium dynamics. *J. Phys. Condens. Matter* **16**, S715–S722 (2004).
- 9 Frauenfelder, H., Sligar, S. G. & Wolynes, P. G. The energy landscapes and motions of proteins. *Science* **254**, 1598–1603 (1991).
- 10 Zou, L. N. Spectral responses in granular compaction. *Phys. Rev. E* **81**, 031302-1-14 (2010).
- 11 Parker, A. & Normand, V. Glassy dynamics of gelatin gels. *Soft Matter* **6**, 4916–4919 (2010).
- 12 Lange, R. F. M., Van Gurp, M. & Meijer, E. W. Hydrogen-bonded supramolecular polymer networks. *J. Polym. Sci. Pol. Chem.* **37**, 3657–3670 (1999).
- 13 Feldman, K. E., Kade, M. J., Meijer, E. W., Hawker, C. J. & Kramer, E. J. Model transient networks from strongly hydrogen-bonded polymers. *Macromolecules* **42**, 9072–9081 (2009).
- 14 Noro, A., Matsushita, Y. & Lodge, T. P. Thermoreversible supramacromolecular ion gels via hydrogen bonding. *Macromolecules* **41**, 5839–5844 (2008).
- 15 Sakamoto, A., Ogata, D., Shikata, T., Urakawa, O. & Hanabusa, K. Large macro-dipoles generated in a supramolecular polymer of N,N',N''-tris(3,7-dimethyloctyl) benzene-1,3,5-tricarboxamide in n-decane. *Polymer* **47**, 956–960 (2006).
- 16 Jeffrey, G. A. *An Introduction to Hydrogen Bonding* (Oxford University Press, New York, 1997).
- 17 Semenov, A. N. & Rubinstein, M. Thermoreversible gelation in solutions of associative polymers. 1. Statics. *Macromolecules* **31**, 1373–1385 (1998).
- 18 Rubinstein, M. & Semenov, A. N. Thermoreversible gelation in solutions of associating polymers. 2. Linear dynamics. *Macromolecules* **31**, 1386–1397 (1998).
- 19 Minsk, L. M., Priest, W. J. & Kenyon, W. O. The alcoholysis of polyvinyl acetate. *J. Am. Chem. Soc.* **63**, 2715–2721 (1941).
- 20 Moritani, T. & Fujiwara, Y. C-13-NMR and H-1-NMR investigations of sequence distribution in vinyl alcohol vinyl acetate copolymers. *Macromolecules* **10**, 532–535 (1977).

- 21 Isasi, J. R., Cesteros, L. C. & Katime, I. Hydrogen-bonding and sequence distribution in poly(vinyl acetate-co-vinyl alcohol) copolymers. *Macromolecules* **27**, 2200–2205 (1994).
- 22 Urakawa, O., Ikuta, H., Noubukawa, S. & Shikata, T. Small-angle neutron scattering study on the miscibility and concentration fluctuation of hydrogen-bonded polymer blends. *J. Polym. Sci. Pol. Phys.* **46**, 2556–2565 (2008).
- 23 Coleman, M. M., Graf, J. F. & Painter, P. C. *Specific Interactions and the Miscibility of Polymer Blends* (Technomic, Lancaster, PA, 1991).
- 24 Ferry, J. D. *Viscoelastic Properties of Polymers* 4th edn (Wiley, New York, 1980).
- 25 Fecko, C. J., Eaves, J. D., Loparo, J. J., Tokmakoff, A. & Geissler, P. L. Ultrafast hydrogen-bond dynamics in the infrared spectroscopy of water. *Science* **301**, 1698–1702 (2003).
- 26 Debenedetti, P. G. & Stillinger, F. H. Supercooled liquids and the glass transition. *Nature* **410**, 259–267 (2001).
- 27 Parisi, G. & Sciortino, F. Structural glasses flying to the bottom. *Nat. Mater.* **12**, 94–95 (2013).

Supplementary Information accompanies the paper on Polymer Journal website (<http://www.nature.com/pj>)